

Maximum Likelihood Doppler Frequency Estimation Under Decorrelation Noise for Quantifying Flow in Optical Coherence Tomography

Aaron C. Chan, *Student Member, IEEE*, Vivek J. Srinivasan*, and Edmund Y. Lam, *Senior Member, IEEE*

Abstract—Recent hardware advances in optical coherence tomography (OCT) have led to ever higher A-scan rates. However, the estimation of blood flow axial velocities is limited by the presence and type of noise. Higher acquisition rates alone do not necessarily enable precise quantification of Doppler velocities, particularly if the estimator is suboptimal. In previous work, we have shown that the Kasai autocorrelation estimator is statistically suboptimal under conditions of additive white Gaussian noise. In addition, for practical OCT measurements of flow, decorrelation noise affects Doppler frequency estimation by broadening the signal spectrum. Here, we derive a general maximum likelihood estimator (MLE) for Doppler frequency estimation that takes into account additive white noise as well as signal decorrelation. We compare the decorrelation MLE with existing techniques using simulated and flow phantom data and find that it has better performance, achieving the Cramer-Rao lower bound. By making an approximation, we also provide an interpretation of this method in the Fourier domain. We anticipate that this estimator will be particularly suited for estimating blood flow in *in vivo* scenarios.

Index Terms—Circulant matrices, Cramer-Rao bounds, Doppler optical coherence tomography, frequency estimation, maximum likelihood estimation, Toeplitz matrices.

I. INTRODUCTION

A RECENT trend in optical coherence tomography (OCT) hardware development is to increase the A-scan acquisition rate [1], [2], making new *in vivo* applications possible [3], [4]. However, the increase in speed does not necessarily enhance the capabilities of functional OCT imaging. For example, the minimum detectable Doppler shift and blood velocity are not

only determined by the sampling rate, but also by the noise statistics and the estimation method [5]. Estimation performance is determined by the mean squared error (MSE) of the estimator. In this work, we develop a general maximum likelihood estimator for estimating the axial blood flow velocity via the Doppler frequency [5] that takes into account spectral broadening due to decorrelation [6], in addition to the effects of additive white noise.

In our previous work, we examined the statistical performance of frequency estimators [5], [7], [8] for use in Doppler OCT [9]–[11], under additive noise assumptions. Under additive white noise conditions, the Kasai estimator [7] is statistically suboptimal, but can still perform adequately in the presence of moderate amounts of decorrelation noise [12]. The additive white Gaussian noise (AWGN) maximum likelihood estimator (MLE), on the other hand, is statistically optimal for additive white noise conditions and achieves the Cramer-Rao lower bound (CRLB) for moderate SNRs and data lengths. However, even small amounts of decorrelation noise can cause its performance to be worse than that of the Kasai estimator. Hence, the AWGN MLE is only suitable when additive noise dominates decorrelation over the total acquisition time [13].

The effects of decorrelation are expected to increase with acquisition time, particularly when imaging vasculature with blood flow [12]. It is desirable to have an MLE that takes this into account, given that the Kasai estimator is nonparametric and statistically suboptimal [5]. In this paper, we extend our statistical analysis to derive a decorrelation noise MLE that performs better than both the Kasai estimator and AWGN MLE under more general noise conditions.

While decorrelation based techniques such as speckle variance and phase variance are used for the detection of microvasculature, these techniques do not provide quantification of flow [14]–[16]. The estimator we derive incorporates a model of the decorrelation noise [14], to design a better estimator of axial blood velocity, enabling the quantification of slow axial velocities and flow. We compare the decorrelation MLE with the AWGN MLE and the Kasai estimator using simulated data and red blood cell flow phantom data.

II. ADDITIVE WHITE GAUSSIAN NOISE

A. Signal Model and AWGN Maximum Likelihood Estimator

Shot noise affects all types of optical measurements, and hence our Doppler estimators must take this into account. Here, we outline the derivation of the AWGN MLE, as presented in

Manuscript received November 27, 2013; revised February 18, 2014; accepted February 25, 2014. Date of publication March 11, 2014; date of current version May 29, 2014. This work was supported in part by the Fulbright Scholarship Board, in part by the Lee-Hysan Foundation, in part by the National Institutes of Health (R01NS067050, EB001954 R01), in part by the American Heart Association (11IRG5440002), in part by the Glaucoma Research Foundation Catalyst for a Cure, in part by the Hong Kong Research Grants Council-projects 7138/11E and 7131/12E, and in part by the University Research Committee of The University of Hong Kong project 104002345. *Asterisk indicates corresponding author.*

A. C. Chan is with the Department of Electrical and Electronic Engineering, University of Hong Kong, Pokfulam, Hong Kong, and also with the Biomedical Engineering Department, University of California-Davis, Davis, CA 95616 USA (e-mail: cwachan@eee.hku.hk).

*V. J. Srinivasan is with the Biomedical Engineering Department, University of California-Davis, Davis, CA 95616, USA (e-mail: vjsriniv@ucdavis.edu).

E. Y. Lam is with the Department of Electrical and Electronic Engineering, University of Hong Kong, Pokfulam, Hong Kong (e-mail: elam@eee.hku.hk).

Digital Object Identifier 10.1109/TMI.2014.2309986

TABLE I
SOME FREQUENTLY USED SYMBOLS

Symbol	Meaning
Ω_D	Analog Doppler frequency
R	Discrete/continuous autocorrelation function
T	Total acquisition time
N	Total number of data points
Δt	T/N , interval between measurements
\angle	Complex argument
r	Reflectance
ϕ_r	Phase of reflectance
\dagger	Hermitian conjugate

our earlier work [5]. If s_n is a single measured datum at time instance n , see Table I, we represent the Doppler OCT data for measuring flow velocity as [5]

$$s_n = |r| \exp[j(n\Omega_D \Delta t + \phi_r)] + z_n. \quad (1)$$

Here, $|r| \exp(j\phi_r)$ is the unknown complex constant reflectance with its associated phase, and $j = \sqrt{-1}$. The time between measurements is $\Delta t = T/N$, where T is the total acquisition time and N is the total number of samples. The additive noise is given by z_n , which is circularly symmetric, complex, Gaussian. That is, each of the real and imaginary parts of z_n are independent and identically Gaussian distributed with zero mean and equal variance, σ^2 .

From this model, as expressed in (1), we can calculate the likelihood of obtaining a measured signal, $\{s_1, \dots, s_N\}$. We showed that the log-likelihood function is given by

$$\begin{aligned} L &= \log[P(\{s_1, s_2, \dots, s_N\} | \Omega_D, \phi_r)] \\ &= -N \log(2\pi\sigma^2) \\ &\quad - \frac{1}{2\sigma^2} \sum_{n=1}^N \left| s_n - |r| \exp \left[j \left(\frac{n\Omega_D T}{N} + \phi_r \right) \right] \right|^2. \end{aligned} \quad (2)$$

With some additional manipulation [5], it can be shown that maximizing the likelihood function is equivalent to choosing the values of the Doppler frequency, Ω_D , and reflectance phase, ϕ_r , that maximizes the real part of the inverse DFT of the (complex conjugate of the) signal [5]

$$\begin{aligned} & \left(\hat{\Omega}_{D,MLE} \quad \hat{\phi}_{MLE} \right)^T \\ &= \arg \max_{\Omega_D, \phi_r} \left(\operatorname{Re} \left\{ |r| \sum_{n=1}^N s_n^* \exp \left[j \left(\frac{n\Omega_D T}{N} + \phi_r \right) \right] \right\} \right). \end{aligned} \quad (3)$$

As ϕ_r is chosen to make the expression in curly brackets real, finding $\hat{\Omega}_{MLE}$ is equivalent to finding the frequency corresponding to the peak of the power spectral density, as illustrated in Fig. 1. This method is also the basis for the joint spectral and time domain OCT (STdOCT) method of Szkulmowski and Szkulmowska [9], [10]. As the AWGN MLE is parametric, provided that the acquired signal is well described by the noise model, it is asymptotically efficient and unbiased [17]. However, its performance may deteriorate in the presence of outliers or deviations from model assumptions, such as in the presence of decorrelation noise, as shown in [5].

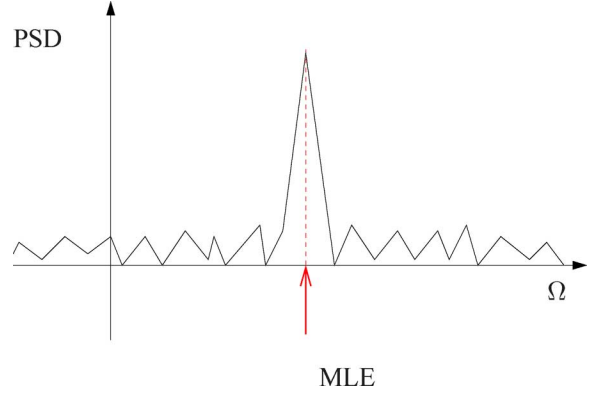


Fig. 1. AWGN MLE for Doppler frequency is the location of the peak of the PSD [5]. Compare this with the decorrelation MLE (Fig. 7).

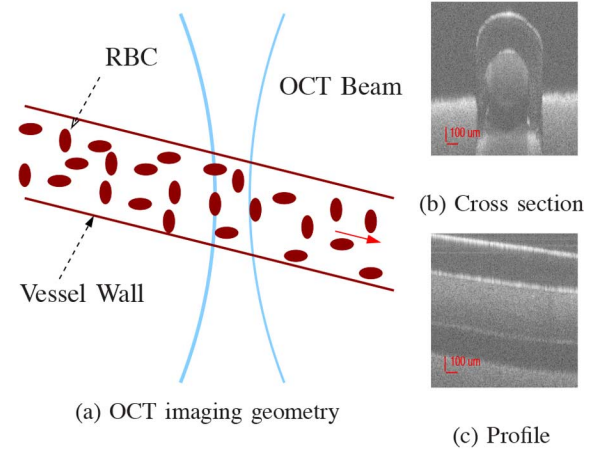


Fig. 2. Schematic diagram of OCT measurement of blood flow. The axial velocity of the red blood cells is measured by the Doppler shift. The changing configuration of scatterers over time causes decorrelation. (b) Cross section and (c) profile of flow phantom experimental set-up. The tubing was tilted at approximately 10° to the horizontal. A-lines were taken down the middle of the tubing.

B. AWGN Cramer-Rao Lower Bound

The theoretical best performance of an unbiased estimator is given by the CRLB. Hence an understanding of this bound would help one to understand the fundamental statistical limits of estimation under a certain type of noise. We showed in [5] that the AWGN MLE achieves the CRLB for realistic SNRs in OCT. The CRLB for an estimator assuming AWGN is given by [5]

$$\operatorname{Var}(\hat{\theta}_1) = \operatorname{Var}(\hat{\Omega}_D) \geq \frac{12N\sigma^2}{(N^2 - 1)|r|^2 T^2}. \quad (4)$$

For large N , the CRLB can be approximated as

$$\operatorname{Var}_{CR}(\hat{\Omega}_D) \approx \frac{12\sigma^2}{N|r|^2 T^2}. \quad (5)$$

Here the CRLB, for a large number of samples N , is inversely proportional to N . It is also inversely proportional to the SNR, $|r|^2/2\sigma^2$, and inversely proportional to the square of the total acquisition time T . By assuming a constant rate of detected

photons (power), the shot-noise limited SNR is proportional to $\Delta t = T/N$. Under these conditions

$$\text{Var}_{\text{CR}}(\hat{\Omega}_{\text{D}}) \sim 1/T^3. \quad (6)$$

Thus, in this limit, the CRLB has the intuitive property of being inversely proportional to the cube of the total acquisition time. As the total number of photons detected is proportional to T , an additional factor of $1/T^2$ arises because the variance of the spectrum is proportional to $1/T^2$. More importantly for large N , the CRLB becomes independent of N . As the MLE variance approaches the CRLB asymptotically, we can infer that for sufficiently large N , the MLE variance also becomes independent of sampling rate.

We argued that the minimum detectable Doppler shift is related to estimator standard deviation [5] for an unbiased estimator. The minimum estimator standard deviation is given by the square root of the CRLB

$$\Omega_{\text{min}} \approx \sqrt{\text{Var}(\hat{\Omega}_{\text{D}})} \equiv \sigma_{\hat{\Omega}_{\text{D}}} \geq \sqrt{\text{Var}_{\text{CR}}(\hat{\Omega}_{\text{D}})}. \quad (7)$$

We conclude that under conditions of AWGN, simply increasing the acquisition rate, $1/\Delta t$, does not reduce the minimum measurable Doppler shift. According to theory, increasing the SNR and increasing the total acquisition time improve the minimum resolvable Doppler shift. However, in reality, it is known that increasing the acquisition time increases the effect of decorrelation noise [5], [18].

III. KASAI ESTIMATOR

Kasai derived an estimator [7] to calculate Doppler shifts of continuous wave ultrasound signals. While derived for processing analog signals, it is often utilized in its discrete form for OCT. The phase, \angle , of the estimated lag one autocorrelation function acts as an estimate of the phase change during this time interval. From this one obtains an estimate for the Doppler frequency, given by

$$\begin{aligned} \hat{\Omega}_{\text{Kasai}} &= \frac{\angle \left(\sum_{n=1}^{N-1} s_{n+1} s_n^* \right)}{\Delta t} \\ &= \frac{\angle \left\{ \sum_{n=1}^{N-1} |s_{n+1}| |s_n| \exp[j(\phi_{n+1} - \phi_n)] \right\}}{\Delta t}. \end{aligned} \quad (8)$$

Here, s_n is the signal acquired at the n th time instance, ϕ_n , its phase, and Δt , the time between measurements. We have discussed in [5] that as a nonparametric estimator, it is not optimized for any specific noise model [12].

IV. DECORRELATION NOISE

A. Decorrelation Noise and Signal Model

It is well known that *in vivo* OCT signals contain decorrelation noise [12], and this needs to be accounted for in any effective parametric estimation scheme [19]. Consider a stationary OCT beam such that a voxel is imaging a blood vessel. At any time instant, there are scatterers randomly distributed

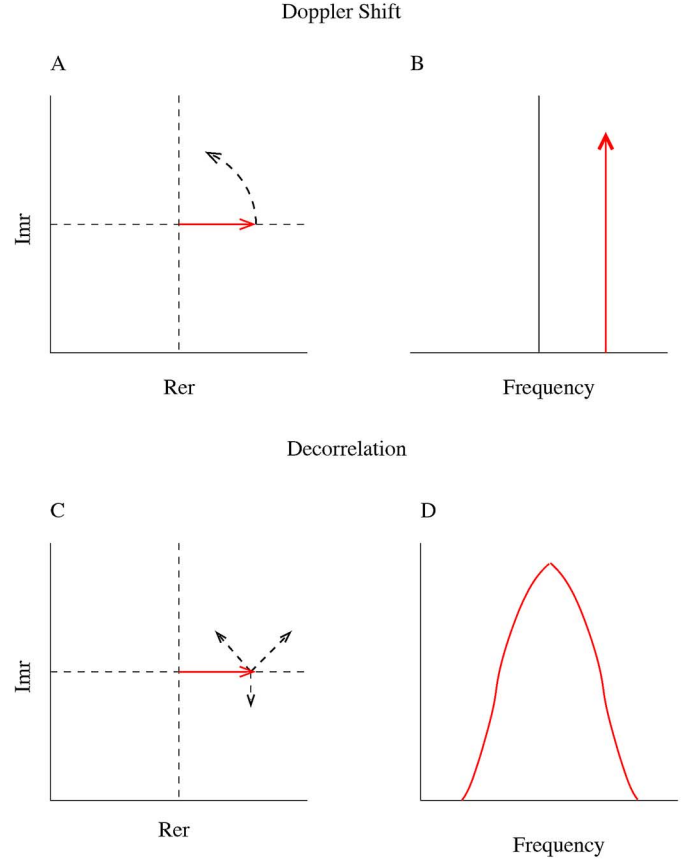


Fig. 3. Doppler shifts shift the PSD, whereas decorrelation broadens the PSD [20]. For high flows rates at angles nearly perpendicular to the OCT beam, one would observe small Doppler shifts, but large spectral broadening. Hence, there is a need for a decorrelation noise MLE.

within the voxel. As the scatterers move into and out of a voxel, the configuration of scatterers changes, and the signal “decorrelates,” as illustrated in Fig. 2. This corresponds to a relaxation of the auto-covariance function, and leads to the broadening of the power spectral density (PSD), as shown in Fig. 3. We simulated decorrelation using Doppler shifted correlated random variables. Hence, the signal is obtained by modifying the signal from (1) to include a (unitless) multiplicative term q_n

$$s_n = q_n |r| \exp[j(n\Omega_{\text{D}}\Delta t)] + z_n \quad (9)$$

where q_n is a correlated complex Gaussian random variable with a known auto-covariance matrix, Σ , and unit amplitude. The covariance matrix Σ is real and Toeplitz symmetric, with the first row equal to the auto-covariance function. Its $1/e$ half-width, τ , is the coherence time of the signal. As Fig. 4 shows, the coherence time decreases as the speed of the red blood cell flow phantom increases. To model this spectral broadening in simulation, the auto-covariance matrix may be set to be an implicit function of Ω_{D} . A signal with a long coherence time has little decorrelation noise, whereas a signal with a short coherence time has a high level of decorrelation noise [18].

To generate a series of correlated random variables $\mathbf{q} = (q_1, q_2, \dots, q_N)^T$, we multiply an uncorrelated series of i.i.d (white) Gaussian random variables $\mathbf{w} = (w_1, w_2, \dots, w_N)^T$

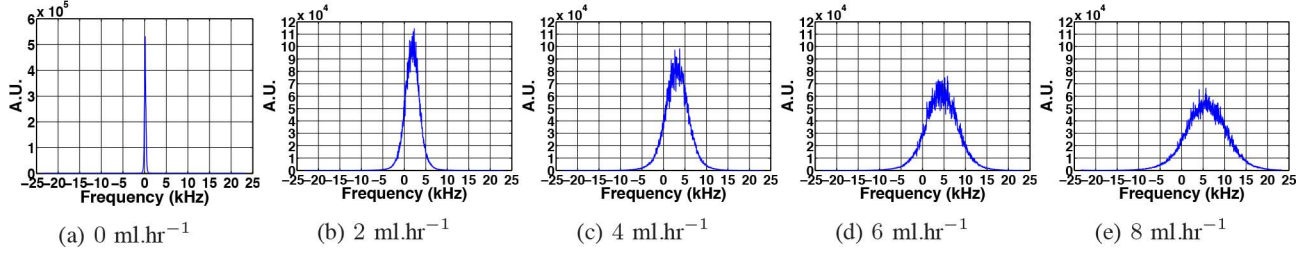


Fig. 4. When power spectra are computed from flow oriented at an angle to the OCT beam at increasing flow rates, the Doppler shift increases with the amount of decorrelation. This figure shows the average PSDs of data collected from rat blood flow phantoms. The averages were taken from 100 repetitions, with a DFT data length of 1024. A cylindrical tubing of diameter 0.58 mm, which was tilted at an angle of elevation of approximately 10° , was used. A flow rate of 8 ml.hr^{-1} corresponds to a average flow speed of roughly 8.4 mm.s^{-1} , and an average axial velocity of 1.46 mm.s^{-1} . The coherence time, estimated from the degree of PSD broadening, for RBC flow ranged from roughly 0.44 ms for 2.0 ml.hr^{-1} to roughly 0.15 ms for 8 ml.hr^{-1} . This corresponds to a time interval of approximately $21\Delta t$ to $7\Delta t$ for a 47 kHz spectral domain OCT system.

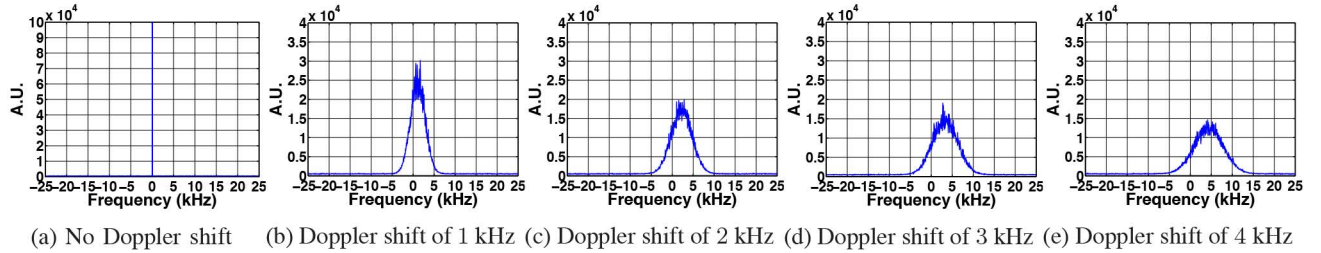


Fig. 5. Data simulated from the signal model in (9) shows the same features of Doppler shift and PSD broadening due to decorrelation as Fig. 4. The coherence time was set to be inversely proportional to the Doppler shift, $1/\tau \propto \Omega_D$ so that PSD widens linearly with Doppler shift as observed experimentally in Fig. 6 and Table II [16], [21]. This figure shows the average PSDs from 100 sets of data simulated from the signal model (9), using a Gaussian covariance matrix, assuming an acquisition time of around 22 ms, and an acquisition rate of 47.0 kHz. The signal to white noise ratio was set to 6 dB. The same data length of 1024 was used for comparing with the OCT signals acquired from RBC flow phantoms.

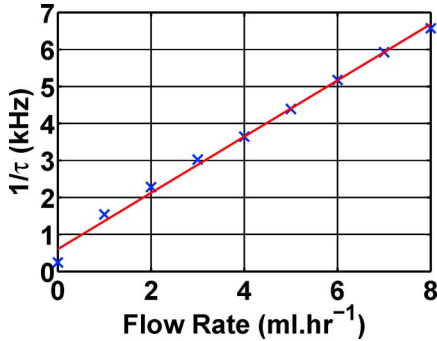


Fig. 6. There is a linear relationship between the broadening of the PSD and the red blood cell flow rate [21], [22].

by the Cholesky decomposition, \mathbf{L} , of the covariance matrix $\mathbf{\Sigma} = \mathbf{L}\mathbf{L}^\dagger$. That is, $\mathbf{q} = \mathbf{L}\mathbf{w}$.

As complex white noise is statistically unchanged under Doppler shifts (it remains white noise), we simplify the expression, (9), by dropping the z_n term and incorporating the effects of white noise into q_n . This can be achieved by modifying the covariance matrix such that all the off diagonal terms are reduced equally by multiplying by $1-\epsilon$. Here, $\epsilon = 1/(1 + \text{SWNR})$, where the signal-to-white-noise ratio (SWNR) is defined by $|r|^2/2\sigma^2$ from (1).

B. Exponential Weighted Covariance Matrix

To gain some insight into the properties of this model, we consider the simple example of an exponential covariance matrix. Though there is experimental evidence to suggest that a

Gaussian covariance matrix better models actual OCT signals [16], as seen in Figs. 4 and 5, this example is computationally more tractable. For a function discretized with step Δt , the exponential covariance matrix is given by

$$\Sigma_{p,q} = \sigma^2 \exp\left(-\frac{|p-q|\Delta t}{\tau}\right). \quad (10)$$

For example, a 4×4 covariance matrix would have the form

$$\mathbf{\Sigma} = \sigma^2 \begin{pmatrix} 1 & x & x^2 & x^3 \\ x & 1 & x & x^2 \\ x^2 & x & 1 & x \\ x^3 & x^2 & x & 1 \end{pmatrix} \quad (11)$$

where $x = \exp(-\Delta t/\tau)$. The inverse of the covariance matrix is tri-diagonal

$$\mathbf{\Sigma}^{-1} = \frac{1}{\sigma^2(1-x^2)} \begin{pmatrix} 1 & -x & 0 & 0 \\ -x & 1+x^2 & -x & 0 \\ 0 & -x & 1+x^2 & -x \\ 0 & 0 & -x & 1 \end{pmatrix} \quad (12)$$

which simplifies calculations in any optimization procedure, and the calculations for the CRLB below. For a very short coherence time $\tau \ll \Delta t$, this reduces to $\mathbf{\Sigma}^{-1} = \mathbf{I}/\sigma^2$.

All covariance matrices of weakly stationary stochastic processes are Toeplitz [23], [24]. To gain insight into the nature of this estimator, it is convenient to approximate the Toeplitz matrices by circulant matrices [25]–[28]. All circulant matrices are diagonalized by the DFT matrix (that is, their eigenvectors are the Fourier bases), and their eigenvalues are given by the DFT

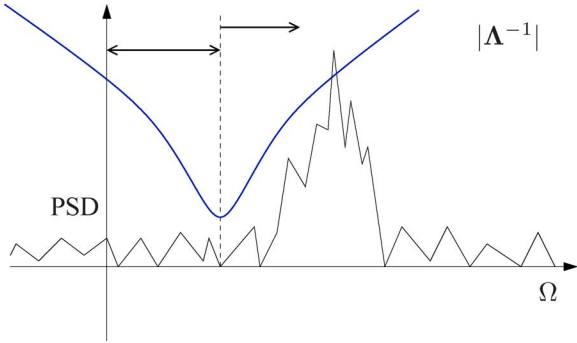


Fig. 7. Circulant approximated decorrelation MLE for Doppler frequency is found by finding the minimum of the convolution of the PSD with the diagonal elements of $|\Lambda^{-1}|$, which is a well centered at the origin. The width of the well is determined by the coherence time. The longer the coherence time the narrower the well. Hence, in the limit where the coherence time is much longer than the acquisition time, the decorrelation MLE performs a similar operation to the AWGN MLE, for the empirically encountered Gaussian or exponential auto-covariance matrices. That is, both the estimators search for the peak of the PSD. A curve fitting or smoothing operation is implicitly incorporated in the decorrelation MLE.

TABLE II
COHERENCE TIMES FOR RED BLOOD CELL FLOW PHANTOM

Flow Rate (ml.hr ⁻¹)	Coherence Time τ (ms)	$1/\tau$ (kHz)
0	4.15	0.241
1	0.65	1.540
2	0.44	2.279
3	0.33	3.024
4	0.27	3.641
5	0.23	4.390
6	0.19	5.175
7	0.17	5.925
8	0.15	6.575

of the first row of the matrix. The inverses of circulant matrices are also circulant.

We construct the circulant approximation, $\mathbf{C} \approx \Sigma$ of the Toeplitz covariance matrix following the example of Gray [26], by setting each row equal to its circularly shifted previous row. This has been proven to be asymptotically equivalent (as the matrix size gets larger) to the Toeplitz covariance matrix in the weak (Hilbert-Schmidt) norm. This approximation is valid, with negligible error for a sufficiently large matrix, when the off diagonal elements are close to zero. In practice, Sherman [29] has shown that for a matrix of size 64×64 , the error, $|\mathbf{s}^\dagger \Sigma^{-1} \mathbf{s} - \mathbf{s}^\dagger \mathbf{C}^{-1} \mathbf{s}|$, would be small if the signal is an AR(1) process (corresponding to an exponential covariance matrix). Under this approximation, the eigenvectors and eigenvalues are asymptotically equivalent [25] to those of the unapproximated covariance matrix. For our decorrelation MLE, the approximation to the covariance matrix would be valid when the coherence time is short, and the matrix is large.

We shall make use of these properties to simplify the decorrelation MLE. This not only reduces the computational complexity, but also provides an intuitive interpretation of the MLE, as show in Fig. 7.

It should be noted that the circulant approximation becomes less accurate for longer coherence times and shorter data lengths [26], as the elements of the covariance matrix in the top right and bottom left are required to be close to zero for the approximation to be accurate.

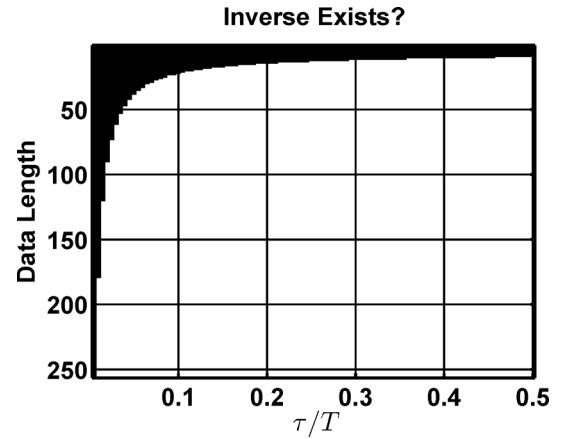


Fig. 8. Invertibility of Gaussian covariance matrices. The top left region (black) of the figure shows where the inverse of the covariance matrices exists. While the matrices are positive definite, for larger matrices, and longer coherence times, the determinant of the matrix approaches zero and becomes numerically noninvertible. This problem can be eliminated by increasing the amount of white noise in the model, which would increase the value of the main diagonal elements relative to off-diagonal elements.

In addition, it should also be noted that when computing the unapproximated decorrelation MLE, in the case of a long coherence time relative to the acquisition time, Gaussian covariance matrices become noninvertible, due to numerical issues caused the early truncation of the covariance function. While the matrix may still be positive definite, the determinant of the matrix approaches zero, as exhibited in Fig. 8.

C. Gaussian Weighted Covariance Matrix

While the exponential-weighted covariance matrix is easier to deal with mathematically, as Fig. 4 shows, actual OCT signals show Gaussian shaped decorrelation [16], [30], [31]. This is due to the Gaussian beam profile in the transverse direction and that the voxel is typically spectrally shaped in processing to be roughly Gaussian in the axial direction

$$\Sigma_{p,q} = \sigma^2 \exp\left(-\frac{|p-q|^2 \Delta t^2}{\tau^2}\right). \quad (13)$$

In our simulations, we have assumed a Gaussian-weighted covariance matrix.

D. Decorrelation Noise MLE in Temporal Domain

We define the vector \mathbf{s} as the signal vector multiplied by a complex exponential of frequency Ω_D

$$\mathbf{s} = \begin{pmatrix} s_1 \exp(-j\Omega_D \Delta t) \\ \vdots \\ s_N \exp(-jN\Omega_D \Delta t) \end{pmatrix}. \quad (14)$$

By setting $z_n = 0$, the likelihood function is given by [13]

$$P(\{s_1, \dots, s_N\} | \Omega_D) = \frac{1}{(2\pi)^N \det(\Sigma)} \exp\left(-\frac{\mathbf{s}^\dagger \Sigma^{-1} \mathbf{s}}{|\tau|^2}\right). \quad (15)$$

Therefore the multiplicative decorrelation MLE for Ω_D is

$$\hat{\Omega}_{\text{dMLE}} = \arg \min_{\Omega} (\mathbf{s}^\dagger(\Omega_D) \mathbf{\Sigma}^{-1} \mathbf{s}(\Omega_D)) \quad (16)$$

where \dagger is the Hermitian conjugate. Maximizing the log-likelihood is equivalent to minimizing the quadratic form $\mathbf{s}^\dagger(\Omega_D) \mathbf{\Sigma}^{-1} \mathbf{s}(\Omega_D)$ with respect to Ω_D . This can be computed using standard optimization algorithms [32]. Note that $\mathbf{\Sigma}$ here is general. It may be Gaussian weighted, if this is known *a priori* [16], or it may be estimated from data.

E. Decorrelation Noise CRLB

Assuming that additive noise is negligible, the log-likelihood function can also be written as

$$L = -\frac{1}{|r|^2} \mathbf{s}^\dagger(\Omega_D) \mathbf{\Sigma}^{-1} \mathbf{s}(\Omega_D) - N \log(2\pi) - \log(\det(\mathbf{\Sigma})). \quad (17)$$

We assume that $\mathbf{\Sigma}$ is independent from, or is merely an implicit function of, Ω_D . From this we can obtain the Fisher information [5] from

$$J(\Omega) = -E \left(\frac{\partial^2 L}{\partial \Omega_D^2} \right) \quad (18)$$

and the CRLB from

$$\text{Var}(\hat{\Omega}_D) \geq \frac{1}{J(\Omega_D)}. \quad (19)$$

For the numerical evaluation of the maximum likelihood using a gradient-based optimization, one may evaluate the gradient by

$$\frac{\partial L}{\partial \Omega_D} = -\frac{1}{|r|^2} \{j \Delta t [\mathbf{s}^\dagger(\mathbf{M} \mathbf{\Sigma}^{-1} - \mathbf{\Sigma}^{-1} \mathbf{M}) \mathbf{s}]\}. \quad (20)$$

To derive the Fisher information, (18)

$$\begin{aligned} \frac{\partial^2 L}{\partial \Omega_D^2} &= \frac{-1}{|r|^2} \left(\frac{\partial^2 \mathbf{s}^\dagger}{\partial \Omega_D^2} \mathbf{\Sigma}^{-1} \mathbf{s} + 2 \frac{\partial \mathbf{s}^\dagger}{\partial \Omega_D} \mathbf{\Sigma}^{-1} \frac{\partial \mathbf{s}}{\partial \Omega_D} + \mathbf{s}^\dagger \mathbf{\Sigma}^{-1} \frac{\partial^2 \mathbf{s}}{\partial \Omega_D^2} \right) \\ &= \frac{(\Delta t)^2}{|r|^2} [\mathbf{s}^\dagger (\mathbf{M}^2 \mathbf{\Sigma}^{-1} - 2 \mathbf{M} \mathbf{\Sigma}^{-1} \mathbf{M} + \mathbf{\Sigma}^{-1} \mathbf{M}^2) \mathbf{s}] \end{aligned} \quad (21)$$

where

$$\mathbf{M} = \begin{pmatrix} 1 & 0 & \cdots & 0 \\ 0 & 2 & \cdots & 0 \\ \vdots & \vdots & \ddots & \vdots \\ 0 & 0 & \cdots & N \end{pmatrix}. \quad (22)$$

Using the properties of the trace operation, the expression (21) can be written as

$$\frac{\partial^2 L}{\partial \Omega_D^2} = \frac{(\Delta t)^2}{|r|^2} \text{Tr}[\mathbf{ss}^\dagger (\mathbf{M}^2 \mathbf{\Sigma}^{-1} - 2 \mathbf{M} \mathbf{\Sigma}^{-1} \mathbf{M} + \mathbf{\Sigma}^{-1} \mathbf{M}^2)]. \quad (23)$$

Hence, the Fisher information is given by

$$J(\Omega_D) = -\frac{(\Delta t)^2}{|r|^2} \times \text{Tr}[\mathbf{E}(\mathbf{ss}^\dagger) (\mathbf{M}^2 \mathbf{\Sigma}^{-1} - 2 \mathbf{M} \mathbf{\Sigma}^{-1} \mathbf{M} + \mathbf{\Sigma}^{-1} \mathbf{M}^2)]. \quad (24)$$

This expression can be further simplified, using the result $\mathbf{E}(\mathbf{ss}^\dagger) = |r|^2 \mathbf{\Sigma}$, to

$$J(\Omega_D) = 2(\Delta t)^2 \text{Tr}[\mathbf{\Sigma} \mathbf{M} \mathbf{\Sigma}^{-1} \mathbf{M} - \mathbf{M}^2]. \quad (25)$$

Hence,

$$\text{Var}_{\text{CR}}(\hat{\Omega}_D) = \frac{N^2}{2T^2 \text{Tr}[\mathbf{\Sigma} \mathbf{M} \mathbf{\Sigma}^{-1} \mathbf{M} - \mathbf{M}^2]}. \quad (26)$$

If one considers the case where

$$\mathbf{\Sigma} = \begin{pmatrix} 1 & 1 - \epsilon & \cdots & 1 - \epsilon \\ 1 - \epsilon & 1 & \cdots & 1 - \epsilon \\ \vdots & \vdots & \ddots & \vdots \\ 1 - \epsilon & 1 - \epsilon & \cdots & 1 \end{pmatrix} \quad (27)$$

the signal model would correspond to the case with AWGN, with a SWNR of $(1 - \epsilon)/\epsilon$. Note that $\mathbf{\Sigma}$ is circulant. Fig. 9 confirms that in this case, the decorrelation noise CRLB reduces to that of the AWGN CRLB for sufficiently large SWNRs and N . This suggests that the decorrelation MLE is a more general estimation framework that incorporates the case for AWGN. It can be shown that using this covariance matrix, the decorrelation MLE [(16)] is mathematically equivalent to the AWGN MLE. The argument to be maximized is equal to

$$\begin{aligned} -\mathbf{s}^\dagger \mathbf{\Sigma}^{-1} \mathbf{s} &= -\sum_m \sum_n s_m^* \sigma_{m,n} s_n \exp[j\Omega_D \Delta t(m - n)] \\ &= -\sum_m (a + b) s_m^* s_m \\ &\quad + \sum_{n,m} b s_m^* s_n \exp[j\Omega_D \Delta t(mn - n)] \end{aligned} \quad (28)$$

where $\Sigma_{m,n}^{-1} = \sigma_{m,n}$, the diagonal terms of $\mathbf{\Sigma}^{-1}$ are given by a , and the off-diagonal terms of $\mathbf{\Sigma}^{-1}$ are given by $-b$. It can be shown, using the property that the eigenvalues of a circulant matrix are equal to the DFT of its first row, and that the eigenvalues of the inverse of a matrix are equal to the inverse of the eigenvalues of a matrix

$$a = \frac{1}{\epsilon} \left(1 - \frac{1 - \epsilon}{\epsilon + N(1 - \epsilon)} \right) > 0 \quad (29)$$

and

$$b = \frac{1 - \epsilon}{\epsilon[\epsilon + N(1 - \epsilon)]} > 0. \quad (30)$$

Both terms are greater than zero as $0 < \epsilon < 1$. As only the second term of (28) is a function of Ω_D , maximizing $-\mathbf{s}^\dagger \mathbf{\Sigma}^{-1} \mathbf{s}$ is equivalent to finding Ω_D that maximizes the PSD. Therefore, although the likelihood functions are computed in different ways, the decorrelation MLE under AWGN assumptions performs a mathematically equivalent operation to the AWGN MLE [(3)].

If the covariance matrix is function of τ , and τ is unknown, the parameters to be estimated are given by the vector, $\boldsymbol{\theta} = (\Omega_D, \tau)^T$, and the Fisher information matrix is given by

$$\mathbf{J}_{p,q}(\boldsymbol{\theta}) = -E \left(\frac{\partial^2 L(\mathbf{s}; \boldsymbol{\theta})}{\partial \theta_p \partial \theta_q} \right). \quad (31)$$

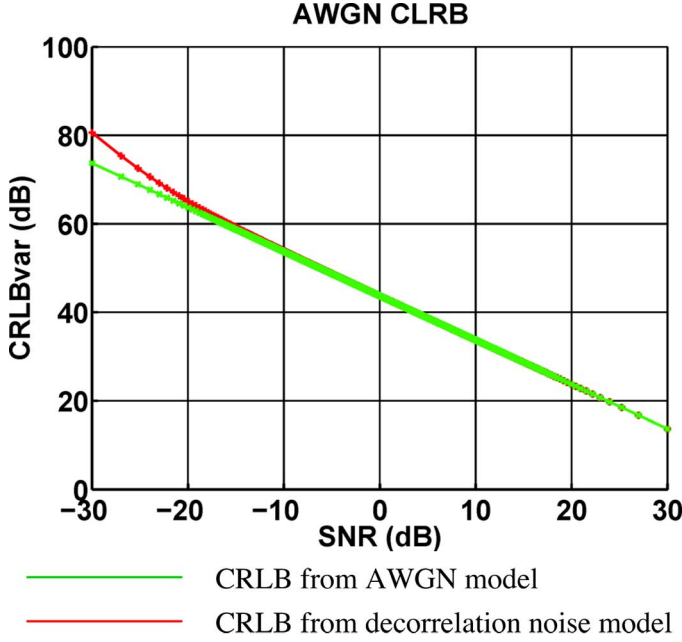


Fig. 9. When computing the CRLB for a signal assuming AWGN and no decorrelation, the values as computed from the decorrelation noise model [(26)] and the AWGN model [(4)] are in agreement. To use the decorrelation noise model CRLB, we assume a covariance matrix as shown in (27) to model AWGN. Here we set $N = 256$ and $T = 0.001$ s. These values are in agreement with the values as computed from the AWGN model [(4)] for experimentally encountered data lengths, N , and SWNRs. It is possible that numerical artifacts occur for low SWNRs, as Σ tends to identity and the denominator in (26) tends to zero. CRLB as computed from the decorrelation noise model [(26)] then deviates to the upside.

The CRLB for the estimator vector $\hat{\theta}$ is then given by

$$\Sigma_{\hat{\theta}} - \mathbf{J}^{-1}(\theta) \geq 0 \quad (32)$$

where $\Sigma_{\hat{\theta}}$ is the covariance matrix of the estimator vector $\hat{\theta}$. As the left hand side is positive semi-definite, the CRLB for the variance of each individual estimator is given by

$$\text{Var}(\hat{\theta}_p) \geq \mathbf{J}_{p,p}^{-1}(\theta). \quad (33)$$

Taking the partial derivative of the log-likelihood with respect to τ twice gives

$$\frac{\partial^2 L}{\partial \tau^2} = -\frac{1}{|r|^2} \mathbf{s}^\dagger(\Omega_D) \frac{\partial^2 \Sigma^{-1}}{\partial \tau^2} \mathbf{s}(\Omega_D). \quad (34)$$

From (20), the off-diagonal terms of the Fisher information matrix are

$$\begin{aligned} \frac{\partial^2 L}{\partial \tau \partial \Omega_D} &= -\frac{j\Delta t}{|r|^2} \left[\mathbf{s}^\dagger \left(\mathbf{M} \frac{\partial \Sigma^{-1}}{\partial \tau} - \frac{\partial \Sigma^{-1}}{\partial \tau} \mathbf{M} \right) \mathbf{s} \right] \\ \frac{\partial^2 L}{\partial \tau \partial \Omega_D} &= -\frac{j\Delta t}{|r|^2} \text{Tr} \left[\mathbf{ss}^\dagger \left(\mathbf{M} \frac{\partial \Sigma^{-1}}{\partial \tau} - \frac{\partial \Sigma^{-1}}{\partial \tau} \mathbf{M} \right) \right] \\ -\text{E} \left(\frac{\partial^2 L}{\partial \tau \partial \Omega_D} \right) &= 0 \end{aligned} \quad (35)$$

as $\text{E}(\mathbf{ss}^\dagger) = |r|^2 \Sigma$ and the trace of three symmetric matrices multiplied together is equal to the trace of any of its permutations. Hence, the value of the CRLB is unchanged regardless of whether τ needs to be estimated or is known *a priori*.

F. Interpretation of Decorrelation Noise MLE in Spectral Domain

By the convolution theorem, multiplying the signal by a complex exponential then taking the DFT is equivalent to shifting the DFT of the signal by the frequency of the sinusoid in the spectral domain

$$\mathcal{F}(\mathbf{s}) = \mathbf{W}\mathbf{s} = \tilde{\mathbf{s}}(\Omega - \Omega_D) \quad (36)$$

where \mathbf{W} is the DFT matrix, and $\tilde{\cdot}$ is the DFT operation. We also know that the circulant covariance matrix is diagonalized by the DFT matrix. By approximating the Toeplitz auto-covariance matrix Σ , by a circulant matrix \mathbf{C} , as defined by Gray [26], (16) then becomes

$$\begin{aligned} \hat{\Omega}_{\text{dMLE}} &= \arg \min_{\Omega} (\mathbf{s}^\dagger(\Omega_D) \Sigma^{-1}(\tau) \mathbf{s}(\Omega_D)) \\ &\approx \arg \min_{\Omega} (\mathbf{s}^\dagger(\Omega_D) \mathbf{C}^{-1}(\tau) \mathbf{s}(\Omega_D)) \\ &= \arg \min_{\Omega} (\mathbf{s}^\dagger(\Omega_D) \mathbf{W}^\dagger \mathbf{\Lambda}^{-1}(\tau) \mathbf{W} \mathbf{s}(\Omega_D)) \\ &= \arg \min_{\Omega} (\tilde{\mathbf{s}}^\dagger(\Omega - \Omega_D) \mathbf{\Lambda}^{-1}(\tau) \tilde{\mathbf{s}}(\Omega - \Omega_D)) \\ &= \arg \min_{\Omega} (\text{Tr} [\mathbf{\Lambda}^{-1}(\tau) \tilde{\mathbf{s}}(\Omega - \Omega_D) \tilde{\mathbf{s}}^\dagger(\Omega - \Omega_D)]). \end{aligned} \quad (37)$$

This approximation can be made if the matrices are close in the weak (Hilbert–Schmidt) norm. As the diagonal entries of $\tilde{\mathbf{s}}(\Omega - \Omega_D) \tilde{\mathbf{s}}^\dagger(\Omega - \Omega_D)$ are the entries of the Doppler shifted PSD, the MLE is equivalent to shifting the spectrum of the data until its weighted inner product (weighted norm) is minimized. The weights are determined by the eigenvalues of the approximated covariance matrix \mathbf{C} , which are determined by the DFT of the covariance function. Empirically observed auto-covariance functions are typically monotonically decreasing, such as in the case of Gaussian auto-covariance functions. Hence, the eigenvalues are typically ordered from largest in magnitude to smallest in the first quadrant. Therefore, the diagonals of $|\mathbf{\Lambda}^{-1}|$ typically form a well shape. The spectra are shifted so that the largest values are closest to the origin, as shown in Fig. 7.

Additive white Gaussian noise can affect the minimization procedure for either the approximated or unapproximated decorrelation MLE if it is not appropriately accounted for in the estimation procedure. Therefore, if the power of the white noise is significant, one would be able to take this into account by uniformly reducing the off-diagonal entries in the covariance matrix.

As the eigenvalues of a circulant matrix comprise of the DFT of the first row of the circulant matrix, the MLE is equivalent to finding the minimum of the modulo- N circular convolution, \circledast , between the PSD of the signal and the *reciprocal* of the DFT of the auto-covariance function, as illustrated in Fig. 7

$$\hat{\Omega}_{\text{dMLE}} = \arg \min_{\Omega} (|\text{PSD}(\Omega) \circledast \mathbf{\Lambda}(\Omega)^{-1}|). \quad (38)$$

For the case of AWGN, given in expression (27), Σ is circulant, and the circulant decorrelation MLE is mathematically equivalent to the unapproximated decorrelation MLE.

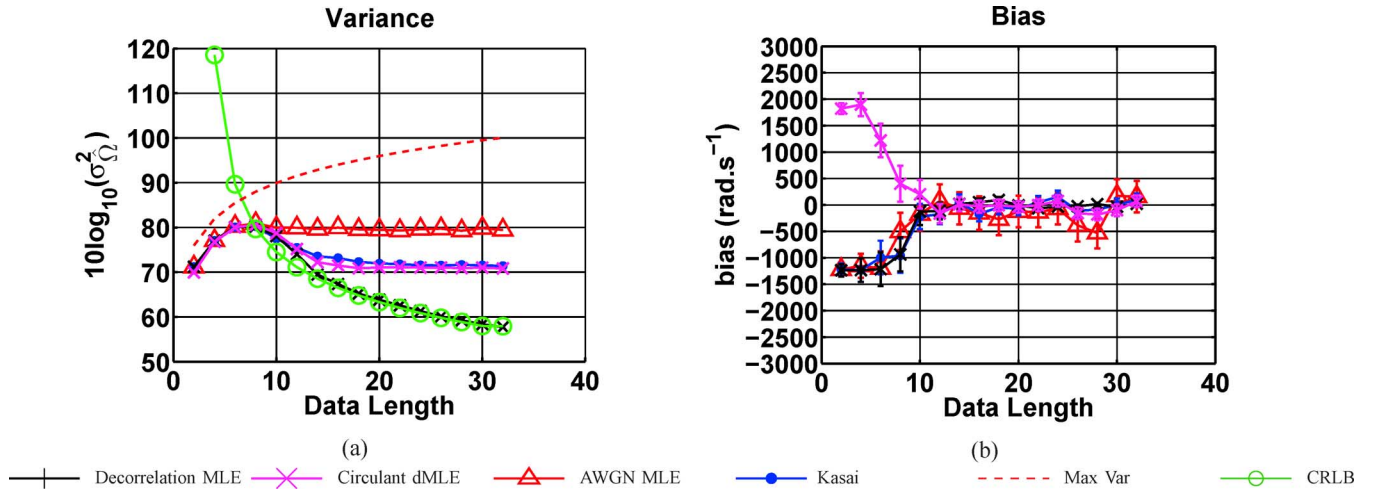


Fig. 10. Increasing the acquisition rate increases the relative performance of the decorrelation noise MLE relative to the other estimators. The decorrelation MLE also achieves the CRLB. This figure shows the estimators under simulated multiplicative decorrelation noise and negligible additive noise against data length for a constant acquisition time. Here, the acquisition time is 1 ms, using 1000 repetitions. A Gaussian weighted covariance matrix was assumed, with a coherence time of 0.10 ms. Hence, $\Delta t/\tau$ ranged from 5.000 down to 0.3125. Higher acquisition rates lead to improved spectral resolution, which improves the decorrelation MLE estimation performance. These conditions represent a relatively large amount of decorrelation, as the coherence time is much shorter than the acquisition time. For short data lengths, the circulant approximated decorrelation MLE has a performance comparable to the unapproximated decorrelation MLE. In addition, for short data lengths, the CRLB is not valid, due to phase wrapping. The maximum variance for an estimator, taking into account phase wrapping, is given by $N^2 \pi^2 / T^2$. (a) Variances are measured in $\text{rad}^2 \cdot \text{s}^{-2}$. (b) Estimator bias in radians per second. When the flows are reversed in simulation, the biases are also reversed.

The general procedure for computing the circulant approximated decorrelation MLE would be as follows.

- Calculate the signal PSD.
- Estimate the covariance function from data.
- Take the DFT of the covariance function. This would give the eigenvalues of the circulant approximation of Σ .
- Take the modulo- N circular convolution of the PSD against the reciprocal of the answer obtained above. Find the minimum of the circular convolution. This is the approximated decorrelation noise MLE (see Fig. 7).

V. ESTIMATION PERFORMANCE

A. Simulation

We ran simulations to estimate the variances and biases of the estimators. The analog frequency was assumed to be $\Omega = 400\pi \text{ rad}\cdot\text{s}^{-1}$ for all simulations, without loss of generality. The simulated acquisition rates were well above the Nyquist limit as the lowest simulated acquisition rate was 2 kHz. Moving scatterers introduce multiplicative decorrelation noise into the signal. Figs. 10 and 11 show that under the presence of multiplicative noise, and negligible additive noise, the decorrelation noise MLE has the best performance, and the AWGN MLE has the worst performance. As the acquisition rate and data length increases, the relative improvement of the decorrelation MLE also increases. Similarly, increasing the coherence time increases the relative performance improvement of the decorrelation MLE.

While the circulant approximation reduced the estimation time, it only shows a marginal improvement of performance over the Kasai estimator. For short acquisition times and coherence times, the circulant approximated decorrelation MLE matched the unapproximated decorrelation MLE. When assuming a Gaussian covariance matrix, it outperformed the

Kasai estimator, but when assuming an exponential covariance matrix, the circulant approximated decorrelation MLE either matched or was slightly worse than the Kasai estimator.

B. Experiment

1) *System Description:* A 1310 nm spectral/Fourier domain OCT microscope was used for the imaging of a flow phantom. The light source consisted of two super-luminescent diodes combined by using a 50/50 fiber coupler to yield a spectral bandwidth of approximately 150 nm. The axial (depth) resolution was $3.6 \mu\text{m}$ (full-width at half-maximum) and the transverse resolution was $7.2 \mu\text{m}$ (full-width at half-maximum), and the highest imaging speed was 47 000 axial scans per second, achieved by an InGaAs line scan camera (Goodrich-Sensors Unlimited, Inc.). The camera sensitivity was typically set to “medium” to obtain the widest dynamic range. The high sensitivity setting typically resulted in a signal saturating the camera pixels. A $5\times$ objective, Mitsutoyo, was used and the center of tubing was placed into focus.

2) *Rat Blood Flow Phantom:* We used rat blood, using heparin as the anticoagulant and a syringe pump with a 0.58 mm inner diameter tubing. The pipe was placed at a 10° incline (approximately), so that there was an axial velocity which could be measured as a Doppler shift. As fluid flow in a tube has a Poiseuille profile, measurements of the Doppler shift were taken at 0.15 mm from the inner edge of the tubing for consistency when making comparisons. Fig. 13 shows that for a $0.1 \text{ ml}\cdot\text{hr}^{-1}$ flow rate, the decorrelation noise MLE has the best performance, whereas the AWGN MLE performed more poorly. While our code was not optimized for speed, for an approximate comparison of computational times, the Kasai algorithm took less than 2 s to generate a 500×100 pixel Doppler map (Fig. 13), with $N = 32$, while the AWGN MLE algorithm took 16 s, and the decorrelation noise MLE took 584 s. The circulant

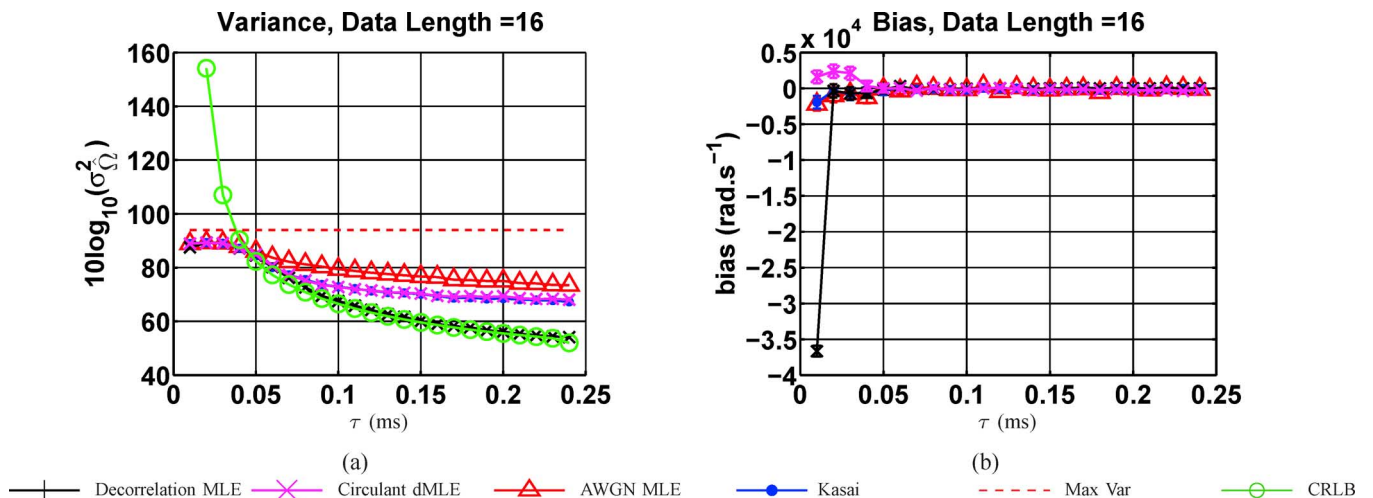


Fig. 11. As the coherence time increases, the relative improvement of performance of the decorrelation MLE against the other estimators also increases. This figure shows the estimators under simulated multiplicative decorrelation noise and negligible additive noise against coherence time in ms. The acquisition time is 1 ms. As the coherence time of the signal decreases, there is more decorrelation. A Gaussian covariance matrix was assumed. The estimation performance of all the estimators decrease as the coherence time decreases, as expected, as the signal becomes more “scrambled.” (a) Variances are measured in $\text{rad}^2 \cdot \text{s}^{-2}$, $N = 16$, using 1000 repetitions. (b) Estimator bias in radians per second.

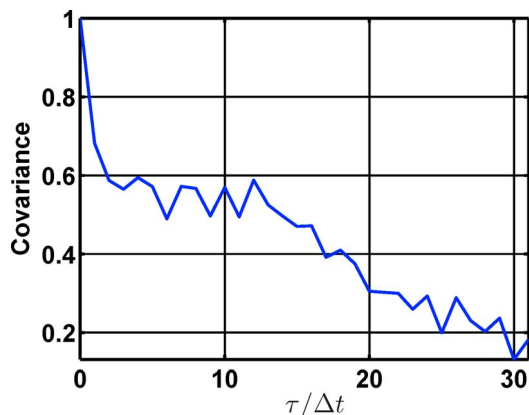


Fig. 12. Absolute value of the normalized covariance function estimated from $0.1 \text{ ml} \cdot \text{hr}^{-1}$ RBC flow phantom data.

approximated decorrelation noise MLE had a similar computation time to the Kasai algorithm when tested on simulated data. This was performed on an Intel Core i7-4800MQ laptop PC running MATLAB R2013a.

To compute the decorrelation MLE, the auto-covariance matrix was estimated from data, by taking the outer product of a data vector with itself, and then averaging over 100 instances (Fig. 12). The DFT length of the AWGN MLE was increased by 256 times using zero padding, so that the estimator variance would not be artifactually rounded to zero.

While the decorrelation noise MLE outperforms the Kasai and AWGN ML estimators, other sources of noise such as galvanometer jitter, thermal drift, and other phase instabilities may affect estimation. As shown in Table II, even at a flow rate of $0 \text{ ml} \cdot \text{hr}^{-1}$, residual decorrelation due to these noises sources is present. Variations in the flow rate could also affect the estimation performance and it is known that blood flow in capillaries can be highly variable [33]. It is known that when trying to estimate high axial velocities fringe washout, which induces

an SNR penalty, may occur [34]–[36]. This would need to be taken into account when making estimates of blood flow. Additionally, if one does not sample at a rate above the Nyquist frequency, phase wrapping would occur. In this paper, however, we are primarily interested in the sensitivity of our Doppler estimates and do not address fringe washout and phase wrapping.

VI. CONCLUSION

In this work, we have derived a multiplicative decorrelation noise MLE that performs better than both the Kasai and AWGN ML estimators under simulated data and flow phantom conditions.

We have also shown that using the appropriate covariance matrix, one can include the effects of additive white noise, and hence the decorrelation noise MLE is more general than the AWGN MLE. Under additive noise only, the AWGN CRLB and decorrelation noise CRLB are asymptotically equivalent for sufficiently large SNRs. The two ML estimators perform mathematically equivalent operations under AWGN assumptions, even though their likelihood functions are derived in different ways.

We have also provided an intuitive interpretation of the decorrelation noise MLE in the Fourier domain, making use of the circulant approximation of Toeplitz matrices. The approximation results in an estimator that is conceptually similar to the PSD centroid estimator described earlier [6], [21]. As the auto-correlation slope at zero time lag is directly related to the PSD centroid [7], the Kasai estimator and circulant approximation to the decorrelation noise MLE have comparable performance.

As the creation of color Doppler maps is easily parallelizable, the decorrelation noise MLE may be implemented on GPUs for faster computation. In addition, one may further speed up the algorithm using gradient-based optimization techniques.

However, challenges remain for the decorrelation noise MLE technique to be applied to *in vivo* situations. When measuring flowing blood and scattering tissue in the same voxel, signals

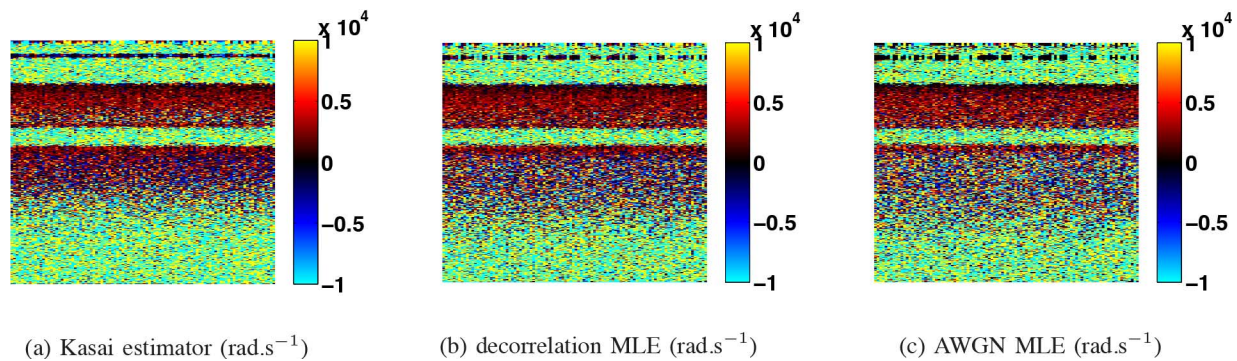


Fig. 13. Color Doppler Maps of $0.1 \text{ ml}\cdot\text{hr}^{-1}$ RBC flow (measurements in $\text{rad}\cdot\text{s}^{-1}$). The acquisition rate was 47 kHz (line scan rate), and the data length was 32 data points. (a) Kasai estimator had a variance of $3.02 \times 10^8 \text{ rad}^2\cdot\text{s}^{-2}$, or 84.8 dB. (b) Decorrelation MLE, where the covariance matrix was estimated from data, had a variance of $1.72 \times 10^8 \text{ rad}^2\cdot\text{s}^{-2}$, or about 2.45 dB better than the Kasai estimate. (c) AWGN MLE has a variance of $5.49 \times 10^8 \text{ rad}^2\cdot\text{s}^{-2}$, which is 2.60 dB worse in performance compared with the Kasai estimator.

would have a large static scattering component, also known as clutter [16], [30], [37]. A static term could thus directly be incorporated into our model to account for clutter. We anticipate a better estimation performance with a better understanding of the scattering properties of RBCs, which would allow more accurate modeling of the underlying biophysical processes. These advances would enable parametric estimation in a wider range of biomedical applications, such as imaging of blood flow in the brain.

ACKNOWLEDGMENT

The authors would like to thank Dr. M. A. Franceschini at the Massachusetts General Hospital for permission to use the OCT system.

REFERENCES

- [1] T. Klein, W. Wieser, L. Reznicek, A. Neubauer, A. Kampik, and R. Huber, "Multi-MHz retinal OCT," *Biomed. Opt. Exp.*, vol. 4, no. 10, pp. 1890–1908, Oct. 2013.
- [2] I. Grulkowski, J. J. Liu, B. Potsaid, V. Jayaraman, C. D. Lu, J. Jiang, A. E. Cable, J. S. Duker, and J. G. Fujimoto, "Retinal, anterior segment and full eye imaging using ultrahigh speed swept source OCT with vertical-cavity surface emitting lasers," *Biomed. Opt. Exp.*, vol. 3, no. 11, pp. 2733–2751, Nov. 2012.
- [3] B. J. Vakoc, D. Fukumura, R. K. Jain, and B. E. Bouma, "Cancer imaging by optical coherence tomography: Preclinical progress and clinical potential," *Nat. Rev. Cancer*, vol. 12, no. 5, pp. 363–368, Apr. 2012.
- [4] V. J. Srinivasan, J. Y. Jiang, M. A. Yaseen, H. Radhakrishnan, W. Wu, S. Barry, A. E. Cable, and D. A. Boas, "Rapid volumetric angiography of cortical microvasculature with optical coherence tomography," *Opt. Lett.*, vol. 35, no. 1, pp. 43–45, Jan. 2010.
- [5] A. C. Chan, E. Y. Lam, and V. J. Srinivasan, "Comparison of Kasai autocorrelation and maximum likelihood estimators for Doppler optical coherence tomography," *IEEE Trans. Med. Imag.*, vol. 32, no. 6, pp. 1033–1042, Jun. 2013.
- [6] J. Walther and E. Koch, "Enhanced joint spectral and time domain optical coherence tomography for quantitative flow velocity measurement," p. 80910L-80910L-7, May 2011.
- [7] C. Kasai, K. Namekawa, A. Koyano, and R. Omoto, "Real-time two-dimensional blood flow imaging using an autocorrelation technique," *IEEE Trans. Sonics Ultrason.*, vol. 32, no. 3, pp. 458–464, May 1985.
- [8] T. Loupas, J. Powers, and R. Gill, "An axial velocity estimator for ultrasound blood flow imaging, based on a full evaluation of the Doppler equation by means of a two-dimensional autocorrelation approach," *IEEE Trans. Ultrason. Ferroelectr. Freq. Control*, vol. 42, no. 4, pp. 672–688, Jul. 1995.
- [9] M. Szkulmowski, A. Szkulmowska, T. Bajraszewski, A. Kowalczyk, and M. Wojtkowski, "Flow velocity estimation using joint spectral and time domain optical coherence tomography," *Opt. Exp.*, vol. 16, no. 9, pp. 6008–6025, Apr. 2008.
- [10] A. Szkulmowska, M. Szkulmowski, A. Kowalczyk, and M. Wojtkowski, "Phase-resolved doppler optical coherence tomography—Limitations and improvements," *Opt. Lett.*, vol. 33, no. 13, pp. 1425–1427, Jul. 2008.
- [11] T. Schmolli, C. Kolbitsch, and R. A. Leitgeb, "Ultra-high-speed volumetric tomography of human retinal blood flow," *Opt. Exp.*, vol. 17, no. 5, pp. 4166–4176, Mar. 2009.
- [12] B. Vakoc, G. Tearney, and B. Bouma, "Statistical properties of phase-decorrelation in phase-resolved Doppler optical coherence tomography," *IEEE Trans. Med. Imag.*, vol. 28, no. 6, pp. 814–821, Jun. 2009.
- [13] A. C. Chan, E. Y. Lam, and V. J. Srinivasan, "Doppler frequency estimators under additive and multiplicative noise," in *Proc. SPIE Opt. Coherence Tomogr. Coherence Domain Opt. Methods Biomed. XVII*, Feb. 2013, vol. 8571.
- [14] J. M. Schmitt, S. H. Xiang, and K. M. Yung, "Speckle in optical coherence tomography," *J. Biomed. Opt.*, vol. 4, no. 1, pp. 95–105, Jan. 1999.
- [15] M. S. Mahmud, D. W. Cadotte, B. Vuong, C. Sun, T. W. H. Luk, A. Mariampillai, and V. X. D. Yang, "Review of speckle and phase variance optical coherence tomography to visualize microvascular networks," *J. Biomed. Opt.*, vol. 18, no. 5, p. 050901-050901-13, Apr. 2013.
- [16] V. J. Srinivasan, H. Radhakrishnan, E. H. Lo, E. T. Mandeville, J. Y. Jiang, S. Barry, and A. E. Cable, "OCT methods for capillary velocimetry," *Biomed. Opt. Exp.*, vol. 3, no. 3, pp. 612–629, Mar. 2012.
- [17] E. L. Lehmann and G. Casella, *Theory of Point Estimation*, 2nd ed. New York: Springer-Verlag, 1998.
- [18] I. Cespedes, J. Ophir, and S. Alam, "The combined effect of signal decorrelation and random noise on the variance of time delay estimation," *IEEE Trans. Ultrason. Ferroelectr. Freq. Control*, vol. 44, no. 1, pp. 220–225, Jan. 1997.
- [19] R. Bamler, "Doppler frequency estimation and the Cramer-Rao bound," *IEEE Trans. Geosci. Remote Sens.*, vol. 29, no. 3, pp. 385–390, May 1991.
- [20] V. J. Srinivasan, A. C. Chan, and E. Y. Lam, *Doppler OCT and OCT Angiography for In Vivo Imaging of Vascular Physiology*. Rijeka, Croatia: InTech, Feb. 2012, ch. 2.
- [21] A. Bouwens, D. Szlag, M. Szkulmowski, T. Bolmont, M. Wojtkowski, and T. Lasser, "Quantitative lateral and axial flow imaging with optical coherence microscopy and tomography," *Opt. Exp.*, vol. 21, no. 15, pp. 17711–17729, Jul. 2013.
- [22] A. Bouwens, T. Bolmont, D. Szlag, C. Berclaz, and T. Lasser, "Quantitative cerebral blood flow imaging with extended-focus optical coherence microscopy," *Opt. Lett.*, vol. 39, no. 1, pp. 37–40, Jan. 2014.
- [23] H. Stark and J. W. Woods, *Probability and Random Processes with Applications to Signal Processing*, 3rd ed. Englewood Cliffs, NJ: Prentice-Hall, 2001.
- [24] S. M. Kay, *Fundamentals of Statistical Signal Processing*. Englewood Cliffs, NJ: Prentice-Hall, 1993, vol. 1, Estimation Theory.

- [25] U. Genander and G. Szego, *Toeplitz Forms and Their Applications*. Berkeley, CA: Univ. California Press, 1958.
- [26] R. Gray, "On the asymptotic eigenvalue distribution of toeplitz matrices," *IEEE Trans. Inf. Theory*, vol. 18, no. 6, pp. 725–730, Nov. 1972.
- [27] C. Rino, "The inversion of covariance matrices by finite Fourier transforms (Corresp.)," *IEEE Trans. Inf. Theory*, vol. 16, no. 2, pp. 230–232, Mar. 1970.
- [28] J. Pearl, "On coding and filtering stationary signals by discrete Fourier transforms (Corresp.)," *IEEE Trans. Inf. Theory*, vol. 19, no. 2, pp. 229–232, Mar. 1973.
- [29] P. Sherman, "Circulant approximations of the inverses of Toeplitz matrices and related quantities with applications to stationary random processes," *IEEE Trans. Acoust., Speech, Signal Process.*, vol. 33, no. 6, pp. 1630–1632, Dec. 1985.
- [30] V. J. Srinivasan, S. Sakadžić, I. Gorczynska, S. Ruvinskaya, W. Wu, J. G. Fujimoto, and D. A. Boas, "Quantitative cerebral blood flow with optical coherence tomography," *Opt. Exp.*, vol. 18, no. 3, pp. 2477–2494, Feb. 2010.
- [31] A. C. Chan, E. Y. Lam, and V. J. Srinivasan, "Maximum likelihood estimation of blood velocity using Doppler optical coherence tomography," in *Proc. SPIE Opt. Coherence Tomogr. Coherence Domain Opt. Methods Biomed. XVIII*, Feb. 2014, vol. 8934.
- [32] G. E. Forsythe, M. A. Malcolm, and C. B. Moler, *Computer Methods for Mathematical Computations*. Englewood Cliffs, NJ: Prentice-Hall, 1976.
- [33] D. Kleinfeld, P. P. Mitra, F. Helmchen, and W. Denk, "Fluctuations and stimulus-induced changes in blood flow observed in individual capillaries in layers 2 through 4 of rat neocortex," in *Proc. Nat. Acad. Sci. USA*, Dec. 1998, vol. 95, no. 26, pp. 15741–15746.
- [34] B. White, M. Pierce, N. Nassif, B. Cense, B. Park, G. Tearney, B. Bouma, T. Chen, and J. de Boer, "In vivo dynamic human retinal blood flow imaging using ultra-high-speed spectral domain optical coherence tomography," *Opt. Exp.*, vol. 11, no. 25, pp. 3490–3497, Dec. 2003.
- [35] S. H. Yun, G. Tearney, J. de Boer, and B. Bouma, "Motion artifacts in optical coherence tomography with frequency-domain ranging," *Opt. Exp.*, vol. 12, no. 13, pp. 2977–2998, Jun. 2004.
- [36] J. Walther, G. Mueller, E. Koch, and H. Morawietz, "Signal power decrease due to fringe washout as an extension of the limited doppler flow measurement range in spectral domain optical coherence tomography," *J. Biomed. Opt.*, vol. 15, no. 4, p. 041511-041511-11, Jul. 2010.
- [37] S. Yousefi, Z. Zhi, and R. Wang, "Eigendecomposition-based clutter filtering technique for optical microangiography," *IEEE Trans. Biomed. Eng.*, vol. 58, no. 8, pp. 2316–2323, Aug. 2011.